# Neutrophils promote VLA-4–dependent B cell antigen presentation and accumulation within the meninges during neuroinflammation

Chelsea R. Parker Harp[a], Angela S. Archambault[a], Matthew Cheung[b], Jesse W. Williams[c,1], Rafael S. Czepielewski[c], Patrick C. Duncker[d,e], Aaron J. Kilgore[a], Aidan T. Miller[a], Benjamin M. Segal[d,e,2], Alfred H. J. Kim[b], Gwendalyn J. Randolph[c], and Gregory F. Wu[a,c,3]

[a]Department of Neurology, Washington University in St. Louis, St. Louis, MO 63110; [b]Department of Internal Medicine, Washington University in St. Louis, St. Louis, MO 63110; [c]Department of Pathology and Immunology, Washington University in St. Louis, St. Louis, MO 63110; [d]Holtom-Garrett Family Program in Neuroimmunology, University of Michigan, Ann Arbor, MI 48109; and [e]Multiple Sclerosis Center, Department of Neurology, University of Michigan, Ann Arbor, MI 48109

Edited by Lawrence Steinman, Stanford University School of Medicine, Stanford, CA, and approved October 14, 2019 (received for review June 24, 2019)

**The success of B cell depletion therapies and identification of leptomeningeal ectopic lymphoid tissue (ELT) in patients with multiple sclerosis (MS) has renewed interest in the antibody-independent pathogenic functions of B cells during neuroinflammation. The timing and location of B cell antigen presentation during MS and its animal model experimental autoimmune encephalomyelitis (EAE) remain undefined. Using a new EAE system that incorporates temporal regulation of MHCII expression by myelin-specific B cells, we observed the rapid formation of large B cell clusters in the spinal cord subarachnoid space. Neutrophils preceded the accumulation of meningeal B cell clusters, and inhibition of CXCR2-mediated granulocyte trafficking to the central nervous system reduced pathogenic B cell clusters and disease severity. Further, B cell-restricted very late antigen-4 (VLA-4) deficiency abrogated EAE dependent on B cell antigen presentation. Together, our findings demonstrate that neutrophils coordinate VLA-4–dependent B cell accumulation within the meninges during neuroinflammation, a key early step in the formation of ELT observed in MS.**

B cell | EAE | multiple sclerosis

B cells are uniquely positioned to mediate multiple aspects of central nervous system (CNS) autoimmunity by secreting both pro- and antiinflammatory cytokines, producing antigen-specific Ig, and efficiently capturing and presenting antigen to cluster of differentiation (CD4) T cells. The concept that B cells are integral to the pathogenesis of multiple sclerosis (MS) has been solidified by the recent success of B cell depletion therapy (BCDT) for both relapsing remitting (RRMS) and primary progressive (PPMS) forms of the disease (1–4). Modeling of B cell involvement in MS using experimental autoimmune encephalomyelitis (EAE) has demonstrated the importance of B cell antigen presentation (5). Moreover, EAE studies have revealed the necessity of activation-induced cytidine deaminase (AID) expression and elevated antigen specificity by B cells, indicating a pathogenic role for B cell antigen processing and presentation (5–7).

In MS, the presence of oligoclonal bands (OCBs) within the cerebrospinal fluid (CSF) raises the important question of where cognate B:T cell interactions occur during disease. Ig isolated from the CSF of MS patients are often class-switched to complement-activating IgG subtypes and show signs of affinity maturation, indicative of germinal center (GC) reactions between CD4 T cells and B cells (8). Ongoing cognate interactions within the meninges are supported by the presence of ectopic lymphoid tissue (ELT) in a sizeable fraction of secondary progressive MS (SPMS) patients (9, 10) as well as in mice with various forms of EAE (11–13). The association of both OCBs (14) and ELT (10, 15, 16) with more severe disability in MS patients suggests that antigen-specific B:T cell interactions occurring locally within the CNS compartment participate in the propagation of neuroinflammation. These features of MS also exemplify the importance of compartmental restrictions on B cell-mediated CD4 T cell activation in neuroinflammation and autoimmunity.

The genesis of ELT in autoimmune diseases within the specialized immune CNS compartment is poorly understood. Lehmann-Horn et al. recently found that B cell-specific deficiency in the α4 integrin subunit of very late antigen-4 (VLA-4) reduces susceptibility to active EAE induced by human myelin oligodendrocyte glycoprotein (hMOG) and decreases trafficking of both Th17 CD4 T cells and macrophages to the CNS (17). Fibroblastic reticular cells (FRCs) and chemokines such as CXC chemokine ligand (CXCL13) have been identified as retention factors within the meninges during EAE (11, 15, 18). However, the steps initially involved in creating a suitable meningeal space for B cell traf-

## Significance

**A distinct murine model of multiple sclerosis used to examine factors involved in ectopic lymphoid tissue formation during central nervous system autoimmunity reveals that infiltration and aggregation of B cells within the leptomeninges is dependent upon B cell expression of VLA-4 and is preceded by neutrophil migration. This finding establishes the early mechanisms involved in the establishment of chronic inflammatory changes within the meninges during autoimmune inflammation that promote the formation of ectopic lymphoid tissue associated with disease progression and disability in multiple sclerosis.**

Author contributions: C.R.P.H., J.W.W., R.S.C., A.H.J.K., and G.F.W. designed research; C.R.P.H., A.S.A., M.C., J.W.W., R.S.C., A.J.K., A.T.M., A.H.J.K., and G.F.W. performed research; C.R.P.H., A.S.A., J.W.W., R.S.C., P.C.D., B.M.S., A.H.J.K., G.J.R., and G.F.W. contributed new reagents/analytic tools; C.R.P.H., A.S.A., M.C., J.W.W., R.S.C., P.C.D., A.J.K., A.T.M., B.M.S., A.H.J.K., G.J.R., and G.F.W. analyzed data; and C.R.P.H. and G.F.W. wrote the paper.

The authors declare no competing interest.

This article is a PNAS Direct Submission.



Data deposition: All data discussed in the paper are available via Figshare, https://doi.org/10.6084/m9.figshare.10052051.v1.

[1]Present address: Center for Immunology, University of Minnesota, Minneapolis, MN 55455.

[2]Present addresses: Department of Neurology and The Neurological Institute, The Ohio State University College of Medicine and Wexner Medical Center, Columbus, OH 43210.

[3]To whom correspondence may be addressed. Email: wug@neuro.wustl.edu.

This article contains supporting information online at www.pnas.org/lookup/suppl/doi:10.1073/pnas.1909098116/-/DCSupplemental.

First published November 7, 2019.

ficking and retention, critical for ELT organization within the specialized immune target of the CNS, have yet to be explored.

To examine the unique contributions of B cell antigen-presenting cell (APC) function to CD4 T cell encephalitogenicity, we developed an EAE model allowing for timed onset of disease mediated solely by B cell antigen presentation (6). In conjunction with rapid disease onset, we now describe the formation of large clusters of B cells within the spinal cord subarachnoid space resembling immature ELT. The accumulation of B cells in the spinal cord meninges was preceded by an increase in $CD45^{hi}$, $CD11b^{hi}$, Ly6C-, Gr-1+ myeloid cells. These inflammatory myeloid cells promoted B cell trafficking to the CNS compartment and influenced the formation of pathogenic B cell clusters. Additionally, B cell expression of VLA-4 was necessary for B cell accumulation and the development of passive EAE. These data suggest that neutrophils enhance recruitment or retention of B cells in an anatomic compartment that facilitates B cell access to both antigens and autoreactive T cells.

## Results

**Meningeal Space Is a Niche for B Cells during EAE.** To assess the location where B cells may participate as APCs within the CNS during EAE, we used flow cytometry to assess the frequency of B cells in various CNS tissues. Following immunization of B6 mice with $MOG_{35–55}$, B cells were found in low frequency and detected primarily in the meninges rather than the CNS tissue parenchyma (Fig. 1*A*). A similar frequency and distribution of B cells was observed in the B cell-dependent EAE model involving active immunization of B6 mice with hMOG (Fig. 1*B*), which is unlike an initial assessment of B cell numbers in these models (19). In contrast, passive transfer of MOG-specific encephalitogenic CD4 T cells into B6 mice or mice with selective major histocompatibility complex class II (MHCII) expression by B cells with an elevated precursor frequency of MOG-specific B cells led to a significantly greater frequency of B cells in the CNS. In these passive EAE models, B cells were found in the spinal cord meninges in preponderance to the CNS tissue parenchyma (Fig. 1 *C* and *D*). These results indicate that the meningeal compartment is the primary location where B cells collect during EAE and suggest that, given the proximity to antigenic debris and cognate CD4 T cells, B cells could serve as potent APCs within the meninges.

We previously reported a novel EAE model, in which MHCII expression is induced in a cell-specific as well as temporal manner. B cells are capable of serving all antigen presentation functions during passive EAE as long as the repertoire of B cells

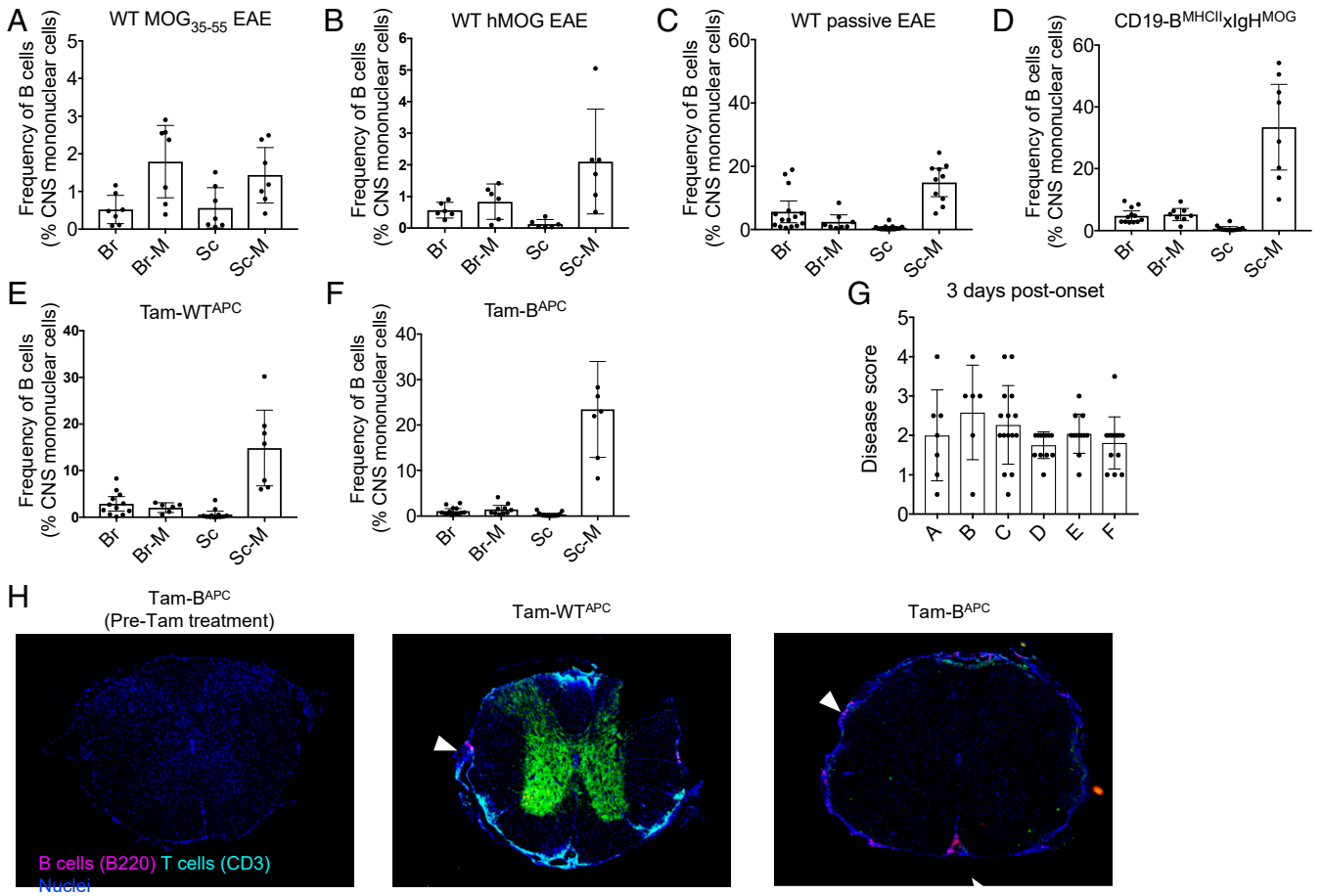


**Fig. 1.** The meningeal space is a niche for B cells during EAE. The mean ± SEM of B cells in different CNS tissues analyzed by flow cytometry. WT mice immunized with (*A*) $MOG_{35–55}$ ($n = 7$, pooled from 2 different experiments) and (*B*) hMOG harvested 3 d post active EAE ($n = 6$, pooled from 2 different experiments). (*C*) WT mice ($n = 15$, pooled from 7 different experiments) and (*D*) CD19-$B^{MHCII}$x$IgH^{MOG}$ mice ($n = 12$, pooled from 4 experiments) harvested 3 d post passive EAE onset. (*E*) Tam-$WT^{APC}$ ($n = 12$, pooled from 5 different experiment) and (*F*) Tam-$B^{APC}$ mice ($n = 13$ mice, pooled from 6 different experiments) treated with Tam 3 wk after CD4 T cell transfer and harvested 3 d post EAE onset. (*G*) Disease severity for samples from *A*–*F* at 3 d postonset. Br, Brain; Br-M, Brain meninges; Sc, Spinal cord; Sc-M, Spinal cord meninges. (*H*) B220 (pink), CD3 (green), and DAPI (blue) immunofluorescence staining of spinal cords carefully excised from recipients of encephalitogenic CD4 T cells. (*Left*) Spinal cord from Tam-$B^{APC}$ mouse harvested 3 wk after T cell transfer without Tam treatment. Spinal cords harvested 3 d post EAE onset from Tam-$WT^{APC}$ (*Middle*) and Tam-$B^{APC}$ (*Right*) mice treated with Tam 3 wk after CD4 T cell transfer. Images are taken at 4× magnification and are representative of $n = 7$ to 8 mice per genotype, pooled from 4 separate experiments. (Scale bars, 100 μm.)

is narrowed on the T cell cognate antigen (MOG) resulting from $IgH^{MOG}$ expression (20). Using this system to examine the critical timing of cognate interactions during neuroinflammation, the onset of disease between Tam-$WT^{APC}$ and Tam-$B^{APC}$ mice can be synchronized by inducing MHCII expression upon oral gavage with Tam after encephalitogenic CD4 T cell transfer (20). We showed that Tam-$WT^{APC}$ mice develop passive EAE similar to WT mice, with or without $IgH^{MOG}$ transgene expression, while Tam-$B^{APC}$ mice can exhibit accelerated disease onset dependent on the timing of MHCII expression relative to encephalitogenic T cell transfer (20). As with other models of EAE, flow cytometric assessment of Tam-$WT^{APC}$ and Tam-$B^{APC}$ mice with EAE revealed infiltration of B cells predominantly within the spinal cord meninges (Fig. 1 *E* and *F*). No significant difference in disease severity was observed between different models at day 3 postonset (Fig. 1*G*). Examination of spinal cord tissue for the presence of B cells in Tam-$WT^{APC}$ and Tam-$B^{APC}$ mice failed to identify evidence of inflammation prior to Tam treatment of mice that had received encephalitogenic CD4 T cells 3 wk prior to harvest. However, B220+ B cells and CD3+ T cells were evident in the spinal cords of Tam-$WT^{APC}$ mice and Tam-$B^{APC}$ mice harvested 3 d post EAE onset, indicating that MHCII+ expression is associated with the induction of lymphocyte trafficking to the CNS (Fig. 1*E*). Interestingly, B cells appeared organized in dense clusters within the meninges in the spinal cord sections from Tam-$B^{APC}$ mice, and this pattern was less common in Tam-$WT^{APC}$ mice (Fig. 1*E*, arrowheads).

**B Cell Clusters with Features of Rudimentary Ectopic Lymphoid Follicles Form in the Spinal Cord of Mice with B Cell-Dependent EAE.** To investigate differences in meningeal B cell clusters in Tam-$B^{APC}$ and Tam-$WT^{APC}$ mice, we quantified the volume and number of B cell clusters. Spinal cords left intact within the spinal column were harvested from mice 3 d after EAE onset, optically cleared, and stained for B cells. Based on this more exhaustive imaging method, B cell staining within the parenchyma of the spinal cord again was rare in both genotypes. Within the meninges, however, small clusters of B cells were observed proximal to the spinal cord of Tam-$WT^{APC}$ mice by confocal imaging (Fig. 2*A*). In contrast, Tam-$B^{APC}$ mice displayed extensive clusters of B220+ B cells that extended several millimeters in length (Fig. 2*B*). Qualitatively, B cell clusters in the meninges of Tam-$B^{APC}$ spinal cords appeared denser than the diffuse B cell infiltration seen in Tam-$WT^{APC}$ mice (Movie S1). Quantifying the area and number of distinct areas of B cell staining in cleared spinal cord specimens, a statistically significant difference in mean voxel area per cluster between the spinal cords of Tam-$WT^{APC}$ ($6857 \pm 1236$) and Tam-$B^{APC}$ mice ($9675 \pm 757$) was observed ($P = 0.05$). Our findings suggest that this model of EAE offers an opportunity to explore the earliest steps involved in B cell organization leading to ELT formation.

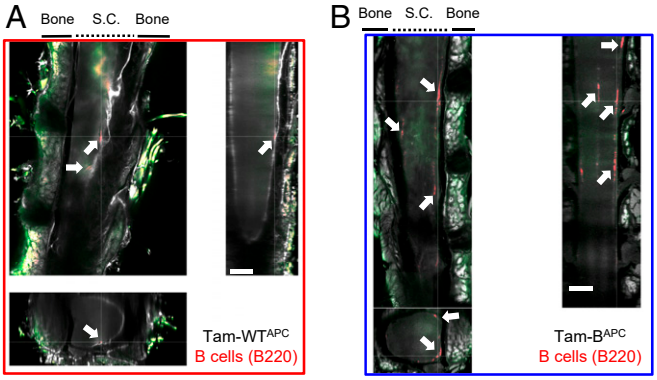


**Fig. 2.** B cells are organized into extensive clusters in Tam-$B^{APC}$ mice. Confocal microscopy of optically cleared spinal cords in vertebrae harvested around 3 d post EAE onset from Tam-$WT^{APC}$ (*A*) and Tam-$B^{APC}$ (*B*) mice that were treated with Tam 3 wk post CD4 T cell transfer. (*Left*) Images show cross-section of *x*, *y*, and *z* axes with cross-hairs centered near B cells. Images show podoplanin+ spinal cord meninges (white), autofluorescent spinal cord parenchyma and bone tissue (green), and B220+ (red) B cells. Images are representative of $n = 4$ cleared spinal cords per genotype, pooled from 3 separate experiments. Arrows indicate B cell clusters. (Scale bar, 500 μm.) S.C., spinal cord.

To gain insight into the resemblance of B cell clusters in the spinal cord meninges to ELT, we first isolated the spinal cord meninges of Tam-$B^{APC}$ mice at 3 d post EAE onset and used flow cytometry to analyze the composition of leukocytes. Splenocytes harvested from an hMOG-immunized mouse were used to develop a gating strategy to detect the expression of GC markers and determine B cell populations present in the meningeal clusters (Fig. 3*A*). Based on expression of IgM and IgD we found that the majority of B cells in the spinal cord meninges included IgM+ IgD− B cells and IgM− IgD− naive mature follicular B cells (Fig. 3*B*). While relatively few B cells existed in the CNS parenchyma, most expressed MHCII. In the spinal cord meninges, where B cells are plentiful, nearly all were MHCII+, indicating a capacity for cognate interactions with CD4 T cells (Fig. 3*C*). CD138+ plasmablasts and plasma cells were very rare in all tissues analyzed but were most frequent in the brain compared to the spinal cord and spinal cord meninges (Fig. 3*C*). The mean frequency of GL7+ GC B cells in the spinal cord meninges was low, although elevated compared to brain and spinal cord parenchyma, indicating that most B cells in the CNS were not undergoing GC-like reactions at this early stage of the disease (Fig. 3*C*). Spinal cord specimens stained with both B220 and the proliferation marker $K_i$-67 revealed the absence of costaining (Fig. 3*D*), demonstrating the formation of B cell clusters just 3 d following the onset of EAE is likely due to a large infiltration of B cells rather than proliferation in situ. Some B cell clusters in the spinal cord meninges were heavily infiltrated by CD3+ T cells (Fig. 3 *E*, *i*, arrows), while T cells were sparse in other clusters (Fig. 3 *E*, *ii*, arrows). In summary, the spinal cord meninges of Tam-$B^{APC}$ mice with EAE rapidly developed dense clusters of activated, class-switched, MHCII+ B cells, suggesting that this is a critical location for cognate interactions during EAE.

To define the specific anatomical site of B cell infiltration within the meninges during EAE, we analyzed decalcified spinal cords harvested from Tam-$B^{APC}$ mice 3 d after EAE onset using immunofluorescent staining. We detected B cell extravasation from the cerebrovasculature which formed clusters surrounding vascular cell adhesion molecule-1 (VCAM-1)+ activated endothelial cells (Fig. 4 *A* and *B*). B cell clusters were excluded from the spinal cord parenchyma, identified by glial fibrillary acidic protein (GFAP) staining (Fig. 4*B*), and pia mater, identified by laminin (Fig. 4*C*). Rather, B cell clusters were associated with the arachnoid mater as seen by Podoplanin-1 staining (Fig. 4 *B* and *C*). Overlays of these immunofluorescent stains revealed that B cell clusters were specifically in the subarachnoid space, an anatomical compartment with access to both antigens and cognate CD4 T cells.

**Inflammatory Myeloid Cells Facilitate B Cell Cluster Formation in the Subarachnoid Space.** The mechanisms of B cell localization to the meninges remain unclear. To understand the kinetics of immune cell trafficking and B cell cluster formation, the spinal cord meninges of Tam-$WT^{APC}$ and Tam-$B^{APC}$ mice harvested at various time points throughout the course of EAE were examined by flow cytometry. The baseline composition of immune cells was measured in Tam-$WT^{APC}$ and Tam-$B^{APC}$ animals harvested 3 wk after receiving encephalitogenic CD4 T cells but prior to Tam

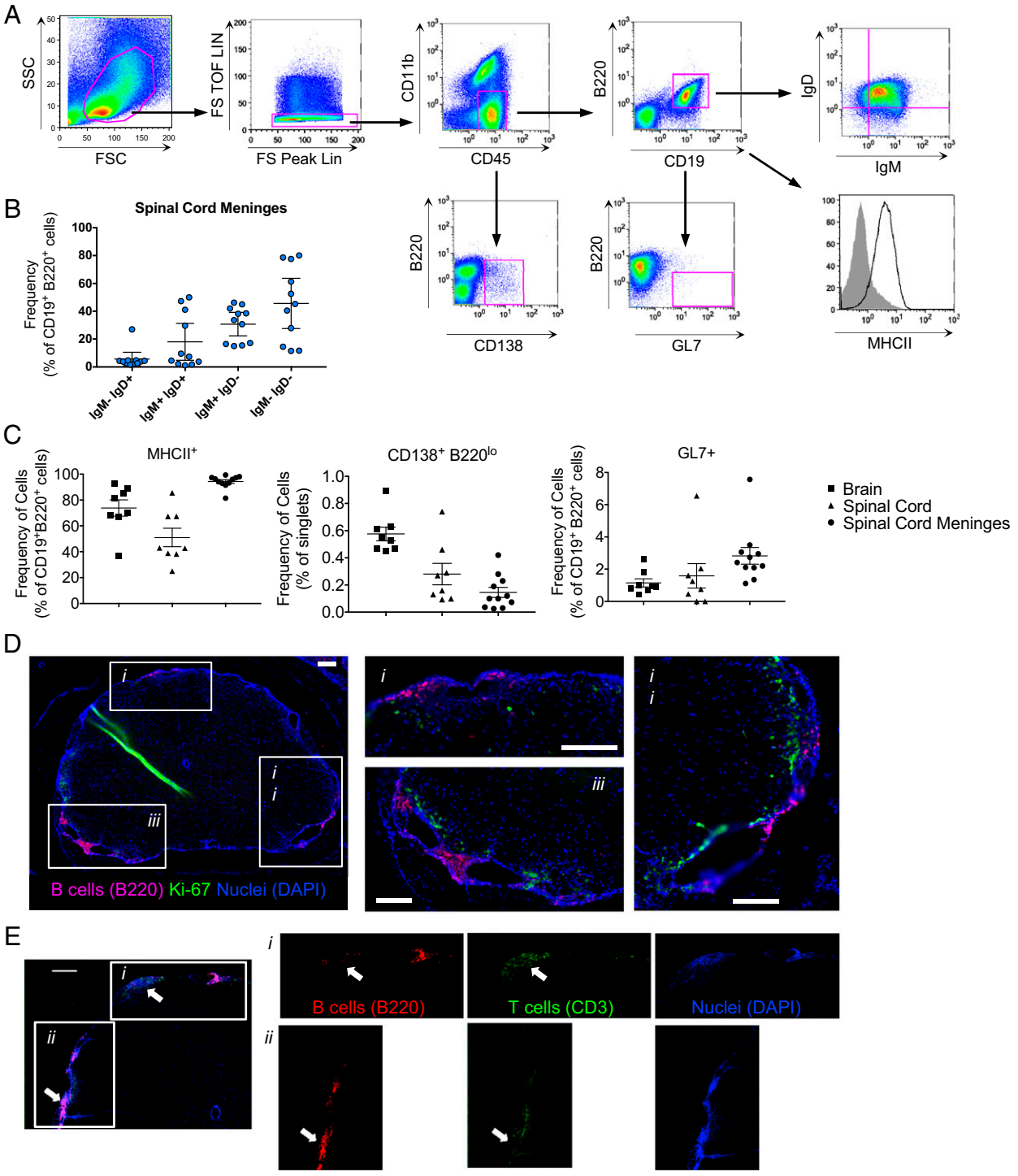


**Fig. 3.** B cell clusters in the spinal cord meninges exhibit features of rudimentary ectopic lymphoid follicles after EAE onset. (*A*) Example flow cytometry gating strategy generated from hMOG-immunized WT splenocytes harvested 3 d post active EAE onset to detect and quantify the data shown in *B* and *C*. Histogram of B cell MHCII staining is overlaid with shaded histogram of CD11b+ cells. (*B*) Frequency of IgM− IgD+ B cells, IgM+ IgD+, IgM+ IgD−, and IgM− IgD− (naive mature follicular B cells) B cells, as a percent of total B cells in the spinal cord meninges of Tam-B$^{APC}$ mice treated with Tam at week 3 post CD4 T cell transfer and harvested around 3 d post EAE onset. Data generated from $n = 11$ mice, pooled from 4 separate experiments. (*C*) Mean frequency with 95% confidence interval of MHCII+ B cells (*Left*) as a percent of total B cells and of CD138+ B220+ plasma cells (*Middle*) and IgD− GL7+ GC B cells (*Right*), out of the total frequency of CNS mononuclear cell singlets in the brain (squares), spinal cord (triangles), and spinal cord meninges (circles) of Tam-B$^{APC}$ mice treated with Tam at week 3 post CD4 T cell transfer and harvested 3 d post EAE onset. Data generated from $n = 11$ mice, pooled from 4 separate experiments. (*D*) B220 (pink), $K_i$-67 (green), and DAPI (blue) immunofluorescence staining of decalcified spinal cord in the vertebrae of Tam-B$^{APC}$ mice treated with Tam at week 3 post CD4 T cell transfer and harvested 3 d post EAE onset. (*Left*) Tam-B$^{APC}$ spinal cord imaged at 4× magnification; boxed *Insets* correspond to 10× magnification of region of interest. Images are representative of $n = 7$ mice, pooled from at least 4 separate experiments. (Scale bars, 100 μm.) (*E*) B220 (red/pink), CD3 (green), and DAPI (blue) immunofluorescence staining of decalcified spinal cord in the vertebrae of Tam-B$^{APC}$ mice treated with Tam at week 3 post CD4 T cell transfer and harvested 3 d post EAE onset. (*i* and *ii*, *Insets*) Single-color images from boxed regions of interest imaged at 10× magnification. Arrows indicate B and T cell colocalization. Images are representative of $n = 7$ mice, pooled from at least 4 separate experiments. (Scale bars, 100 μm.)

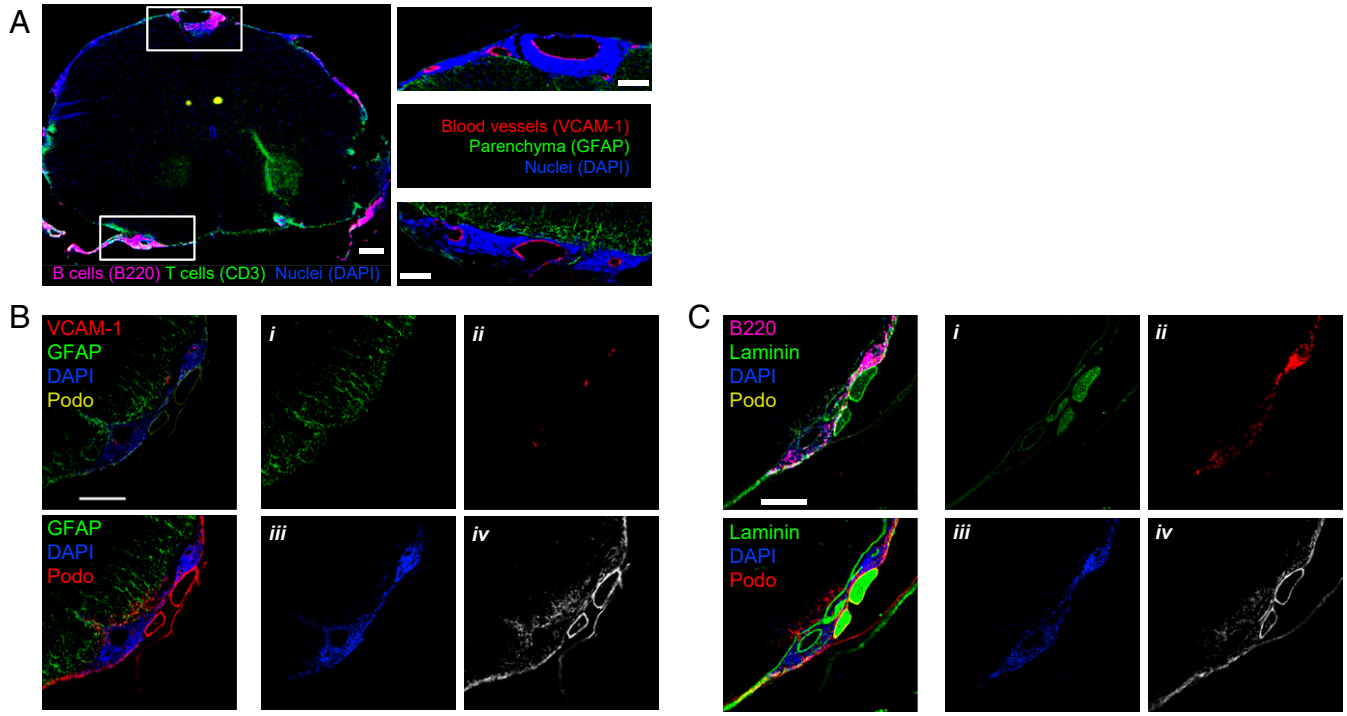


**Fig. 4.** B cell clusters form in the subarachnoid space adjacent to activated endothelial vasculature. Tam-B$^{APC}$ mice were treated with Tam at week 3 post CD4 T cell transfer and killed 3 d post EAE onset. (*A*, *Left*) Decalcified spinal cords were stained for B220 (pink), CD3 (green), and DAPI (blue) and imaged at 4× magnification. (*A*, *Right*) Boxed insets are regions of interest (from left) stained for activated endothelial cells (VCAM-1, red), astrocytes (GFAP, green), and DAPI (blue) and imaged at 10× magnification. (*B*, *Left*, *Top*, and *Bottom*) Overlays of single-color images displayed at *Right*. (*i*) GFAP (green), (*ii*) VCAM-1 (red), (*iii*) DAPI (blue), and (*iv*) podoplanin-1 (white). (*C*) Serial sections of the spinal cord shown in *B*. (*Left*, *Top*, and *Bottom*) Overlay images of single-color images displayed at *Right*. (*i*) Laminin (green), (*ii*) B220 (red), (*iii*) DAPI (blue), and (*iv*) podoplanin-1 (white). All images are representative of $n = 7$ mice, pooled from at least 4 separate experiments. (Scale bars, 100 μm.)



treatment. At 24 and 72 h after induction of MHCII expression, B cell counts were low in the spinal cord meninges of Tam-WT$^{APC}$ mice (Fig. 5*A*) and Tam-B$^{APC}$ mice (Fig. 5*B*). However, by 3 d post EAE onset, B cells were the most numerous cell type analyzed (Fig. 5 *A* and *B*). Donor T cells were virtually undetectable in the spinal cord meninges until the onset of EAE symptoms for Tam-WT$^{APC}$ mice (Fig. 5*A*) and Tam-B$^{APC}$ mice (Fig. 5*B*). Strikingly, we observed early and sustained infiltration of CD45$^{hi}$CD11b$^{hi}$Gr-1$^{hi}$ inflammatory, granulocytic myeloid cells in the spinal cord meninges of Tam-B$^{APC}$ mice but not Tam-WT$^{APC}$ mice, a difference that was statistically significant at 24 h post Tam, 72 h post Tam, and 3 d post EAE onset (Fig. 5*C*). We reasoned that these CD45$^{hi}$CD11b$^{hi}$Gr-1$^{hi}$ inflammatory cells were most likely polymorphonuclear neutrophils (PMNs), as this cell type is rapidly recruited to sites of inflammation and infection and has been detected during initial phases of EAE (21, 22). Imaging of decalcified spinal cords from Tam-B$^{APC}$ mice with EAE revealed the proximity of B cell clusters with Ly6G+ PMNs (*SI Appendix*, Fig. S1), consistent with a coordinated influx of PMNs promoting an environment conducive to B cell antigen presentation and the rapid establishment of B cell clusters following EAE onset.

**Immune Cell Trafficking to the CNS to Induce EAE Is Directed by Distinct Sequences of Chemokine Regulation in WT and B Cell-Dependent EAE.** We reasoned that identification and quantification of the chemokines present in the CSF during the early stages of EAE induction would provide insight into the previously observed differences in the coordinated trafficking of immune cells to the CNS in B cell-dependent EAE. CSF was collected from naive WT mice and pre-Tam Tam-B$^{APC}$ mice, as well as from Tam-WT$^{APC}$ and Tam-B$^{APC}$ mice at 24 and 72 h post Tam, the day of EAE onset, 3 d post EAE onset, and 30 d post Tam to determine the dynamic expression of inflammatory cytokines and chemokines.

The mean concentrations of analytes observed in naive WT mice were similar to the levels detected in CSF collected from Tam-B$^{APC}$ mice harvested 3 wk post CD4 T cell transfer but prior to Tam treatment (Fig. 6 *A*–*E*), indicating that encephalitogenic CD4 T cells did not induce inflammatory responses in the absence of MHCII expression. Tam-WT$^{APC}$ (red squares) exhibited higher concentration of IFNγ at 72 h post Tam compared to Tam-B$^{APC}$ mice ($P = 0.006$). At the day of EAE onset, the concentration in Tam-WT$^{APC}$ mice was still significantly upregulated compared to Tam-B$^{APC}$ mice ($P < 0.0001$) (Fig. 6*A*). Other mediators of inflammation, including CC chemokine ligand (CCL)5 and CCL19 within the CSF CCL5 were significantly different between Tam-WT$^{APC}$ and Tam-B$^{APC}$ mice (Fig. 6 *B* and *C*). Drastically different concentrations of the CXC glutamate-leucine-arginine (ELR)+ chemokines CXCL5, CXCL2, and CXCL1 were identified in the CSF of Tam-WT$^{APC}$ and Tam-B$^{APC}$ mice at the same stages of disease. Tam-WT$^{APC}$ mice tended to rapidly develop much higher concentrations of these chemokines than Tam-B$^{APC}$ mice (Fig. 6*D*).

Given the significance of CXCL13 for B cell trafficking and GC reactions, differences in the concentration of this chemokine between Tam-WT$^{APC}$ and Tam-B$^{APC}$ mice could provide insight into the progression of B cell cluster formation. Although a substantial increase in concentration was observed in both groups, the only difference was identified, at 3 d post EAE onset, with Tam-WT$^{APC}$ mice exhibiting significantly lower CXCL13 concentrations compared to Tam-B$^{APC}$ mice (Fig. 6*E*).

The variability in chemokine concentrations in the CSF between Tam-WT$^{APC}$ mice and Tam-B$^{APC}$ mice, especially at 72 h post Tam, could explain our observation that these 2 genotypes differ in

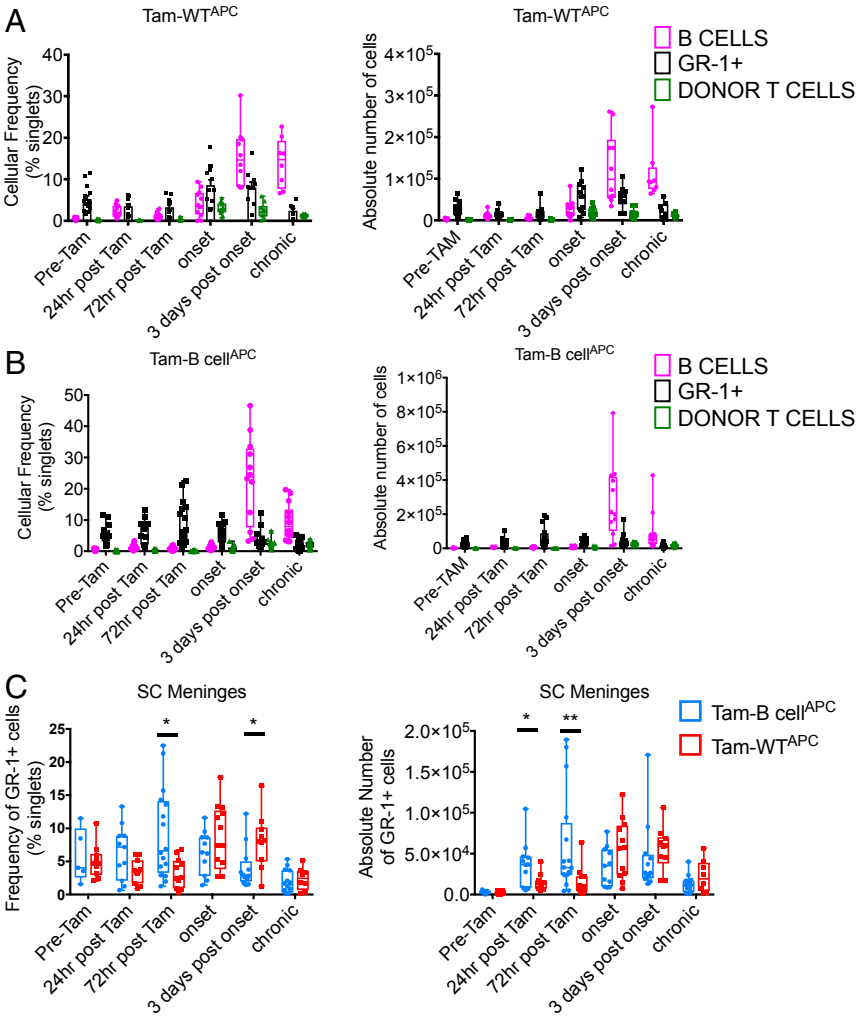


**Fig. 5.** Coordinated trafficking of inflammatory myeloid cells precedes B cell infiltration in B cell-dependent EAE. (*A–C*) Box and whiskers plots showing mean and 10 to 90th percentile data points generated from the frequency (*Left*) and absolute number (*Right*) of B cells (maroon circles), Gr-1+ PMNs (black squares), and donor CD4 T cells (green triangles) in the spinal cord meninges of Tam-B$^{APC}$ mice harvested at 3 wk post T cell transfer and before Tam treatment or from Cre- littermates of Tam-B$^{APC}$ mice harvested at 3 wk post T cell transfer. Data generated from $n = 15$ mice, pooled from at least 4 separate experiments. (*A*) Box and whiskers plots showing mean and min/max data points generated from the frequency (*Left*) and absolute number (*Right*) of B cells (maroon circles), Gr-1+ PMNs (black squares), and donor CD4 T cells (green triangles) in the spinal cord meninges of Tam-WT$^{APC}$ mice harvested at various time points in disease. Data are generated from $n = 8$ to 12 mice per time point, pooled from at least 10 separate experiments. (*B*) Box and whiskers plots showing mean and 10 to 90th percentile data points generated from the frequency (*Left*) and absolute number (*Right*) of B cells (maroon circles), Gr-1+ PMNs (black squares), and donor CD4 T cells (green triangles) in the spinal cord meninges of Tam-B$^{APC}$ mice harvested at various time points in disease. Data generated from $n = 11$ to 16 mice, pooled from at least 10 different experiments. (*C*) Box and whiskers plots showing mean and all data points for frequency (*Left*) and absolute number (*Right*) of Gr-1+ PMNs harvested from the spinal cord meninges of Tam-WT$^{APC}$ mice (red) and Tam-B$^{APC}$ mice (blue) killed at various time points in disease course. Statistical significance was determined by 2-tailed Mann–Whitney *U* tests. Exact *P* values calculated, $*P < 0.05$, $**P < 0.01$.

CD45$^{hi}$CD11b$^{hi}$Gr-1$^{hi}$ inflammatory PMN invasion of the spinal cord meninges (Fig. 5*C*). These ELR+ CXC chemokines all share the receptor CXC chemokine receptor (CXCR)2, which is predominantly expressed by PMNs. In Tam-B$^{APC}$ mice 72 h post Tam, CXCR2 expression was detected in splenic CD45$^{hi}$CD11b$^{hi}$Gr-1$^{hi}$ inflammatory PMN cells, but not on PMNs isolated from the meninges (Fig. 6*F*). However, 3 d post EAE onset, PMN expression of CXCR2 in the spinal cord meninges was notably higher (Fig. 6*F*). B cells did not express CXCR2 in any tissue at any time point examined (Fig. 6*F*). Further flow cytometric analysis of the phenotype of CD45$^{hi}$CD11b$^{hi}$Gr-1$^{hi}$ inflammatory PMNs in the spinal cord meninges of Tam-B$^{APC}$ mice confirmed minimal contamination with Ly6C+ monocytes (*SI Appendix*, Fig. S2). Between 72 h post Tam and 3 d post EAE onset, PMNs isolated from the spinal cord meninges exhibited signs of activation with a reduction in surface expression of CD62L coinciding with increased CXCR2 (*SI Appendix*, Fig. S2). These data are corroborated by reports that transmigration of the blood–brain barrier (BBB) induces enhanced inflammatory phenotypes in PMNs (23). Overall, the data indicate that B cell-dependent EAE promotes a unique inflammatory signaling cascade resulting in the CXCR2-directed recruitment of PMNs at temporally regulated stages of disease.

**Early PMN Recruitment to the CNS Is Required for the Formation of Meningeal B Cell Clusters and Development of EAE.** Modulating CXCR2 signaling with anti-CXCR2 antibodies or small-molecule competitive antagonism has been shown to alter the site of neuroinflammation and the composition of inflammatory infiltrates during EAE and can even modulate the expression of disease symptoms to protect mice from atypical EAE induced by Th17 cells (24, 25). To test whether the early, coordinated recruitment

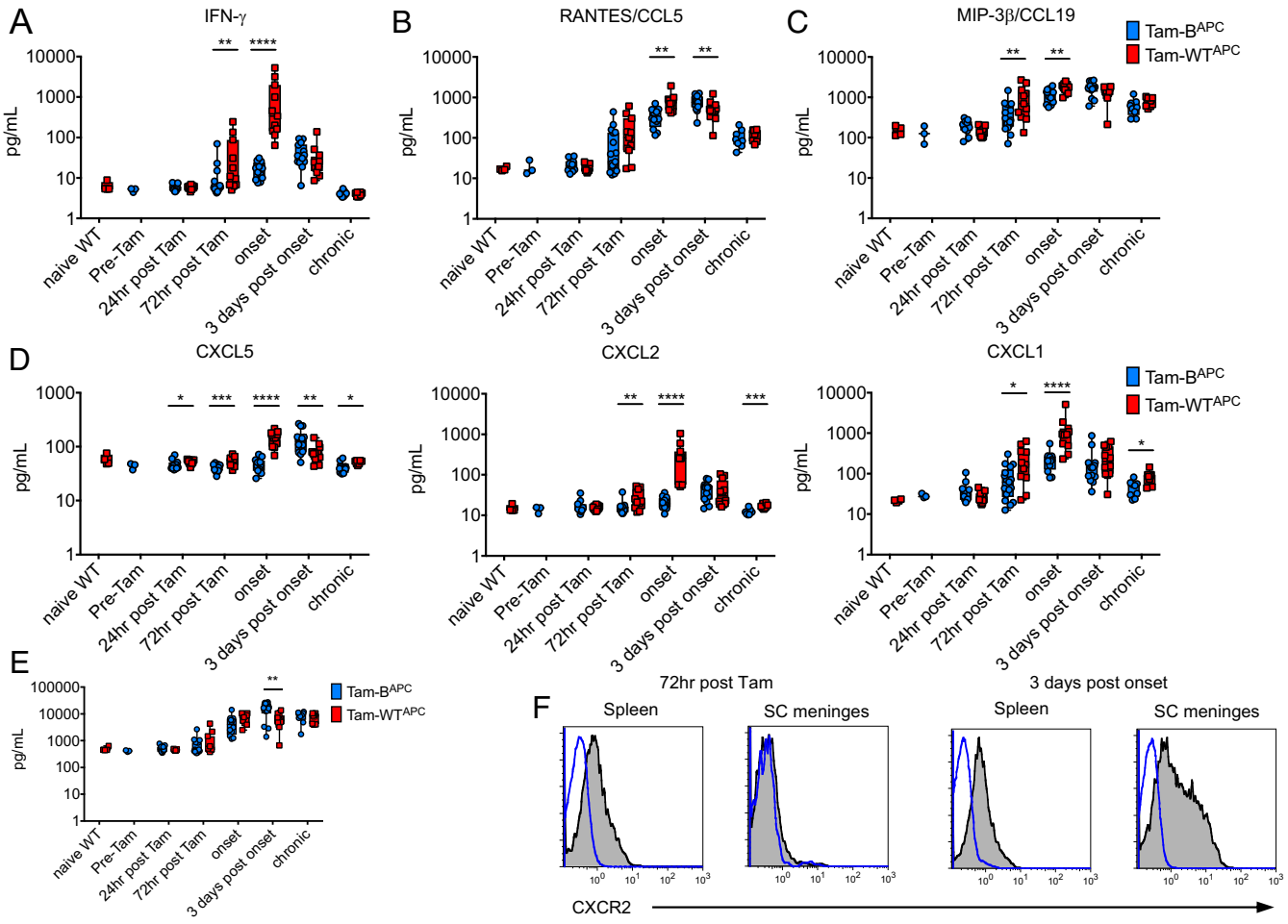


**Fig. 6.** Temporal regulation of chemokine expression mediates immune cell recruitment to the CNS. (*A*–*E*) Graphs show box and whiskers plots with min-to-max error bars of concentrations for (*A*) IFN-γ; (*B*) RANTES/CCL5; (*C*) MIP3-β/CCL19; (*D*) (*Left*) CXCL5, (*Middle*) CXCL2, (*Right*) CXCL1; and (*E*) CXCL13 detected in the CSF of naive WT (black), Tam-WT$^{APC}$ (red) and Tam-B$^{APC}$ (blue) mice harvested at various time points in EAE disease course. Statistical significance was determined by 2-tailed Mann–Whitney *U* tests. Exact *P* values calculated, $*P < 0.05$, $**P < 0.01$, $***P < 0.001$, $****P < 0.0001$. (*F*) Flow cytometric analysis of CXCR2 expression on PMNs (gray histograms) and B cells (blue histograms) isolated from the spleen (*Left*) and spinal cord meninges (*Right*) of Tam-B$^{APC}$ mice collected at 72 h post Tam (*Left* two panels) and 3 d post EAE onset (*Right* two panels). Graphs are representative of $n = 4$ to 5 mice, pooled from 2 separate experiments.

of PMNs to the CNS was functionally relevant to EAE dependent on B cell antigen presentation, we neutralized CXCR2 in Tam-B$^{APC}$ mice. Anti-CXCR2 serum was administered after encephalitogenic CD4 T cells were transferred into Tam-B$^{APC}$ mice but prior to MHCII induction 3 wk later. The disease severity as represented by total area under the curve of mean disease scores was similar for mice receiving control serum and untreated control mice (Fig. 7*A*). Mice treated with anti-CXCR2 blocking antibody did not develop EAE as quickly or as severely as the control groups (Fig. 7*A*). Examination of immunofluorescence images indicates that B cell clusters were present in the spinal cord meninges of both control groups, but were not detected in mice treated with anti-CXCR2 serum (Fig. 7*B*), suggesting that meningeal B cell cluster formation is pathogenic for EAE dependent on B cell antigen presentation. By flow cytometry, donor T cells in the spinal cord meninges of anti-CXCR2–treated mice compared to untreated or control serum groups were similar (*SI Appendix*, Fig. S3 *A* and *B*). As well, B cells and MHCII+ B cells were found in similar numbers in the spleen of anti-CXCR2 mice compared to control groups (*SI Appendix*, Fig. S3*C*). However, in accordance with the absence of meningeal B cell clusters observed 3 d post EAE onset, there were very few B cells in the spinal cord meninges of anti-CXCR2–treated mice (*SI Appendix*, Fig. S3*D*). Our findings suggest that interrupting CXCR2 signaling by PMNs diminished the ability of B cells to access the CNS, a step that may be required for B cell APCs to support EAE.

**B Cell Access to the Subarachnoid Space Is Necessary for B Cell Antigen Presentation to Support Passive EAE.** Based on the observation that EAE was ameliorated and B cell clusters were absent in anti-CXCR2–treated mice, we hypothesized that entry into the CNS compartment was required for B cell antigen presentation to induce neuroinflammation. To test this, CD19-B$^{MHCII}$xIgH$^{MOG}$ and Tam-B$^{APC}$ mice were crossed to mice in which the gene encoding the α4 integrin of the VLA-4 molecule is flanked by LoxP (f/f) sites (VLA-4$^{f/f}$ mice). Protein expression changes were verified in peripheral blood B cells from Tam-B$^{APC}$ mice prior to Tam treatment and 72 h post Tam treatment (Fig. 7*C*). WT and Cre$^{-}$VLA-4$^{f/f}$ mice with WT VLA-4 expression levels were both susceptible to EAE (*SI Appendix*, Table S1) with a similar day of onset and disease severity (Fig. 7 *D*, *Top*). CD19-B$^{MHCII}$xIgH$^{MOG}$ mice and CD19-B$^{MHCII}$xIgH$^{MOG}$xVLA-4$^{f/+}$ mice were susceptible to EAE, but CD19-B$^{MHCII}$xIgH$^{MOG}$xVLA-4$^{f/f}$ mice were completely protected (Fig. 7 *D*, *Center*). We repeated the passive EAE experiment with Tam-B$^{APC}$, Tam-B$^{APC}$xVLA-4$^{f/+}$, and Tam-B$^{APC}$ xVLA-4$^{f/f}$ mice and treated them with Tam at 3 wk post-encephalitogenic CD4 T cell transfer. As expected, mice with WT

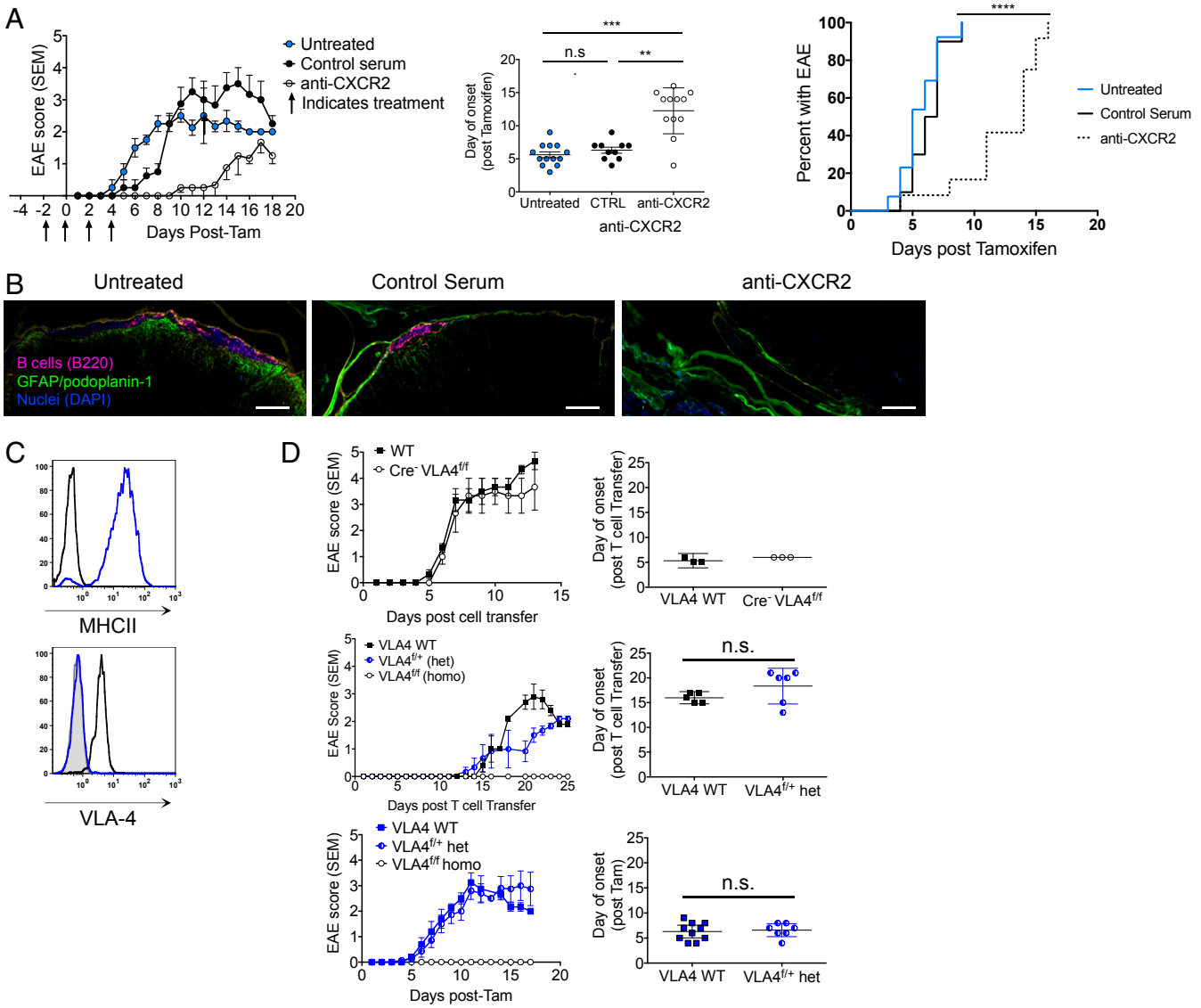


**Fig. 7.** Granulocyte recruitment to the CNS and VLA-4–dependent B cell access to the subarachnoid space are necessary for formation of B cell clusters and B cell antigen presentation to support passive EAE. (*A*) (*Left*) EAE scores ± SEM for Tam-B$^{APC}$ mice from the untreated group (blue circles), control serum group (black circles), and anti-CXCR2 recipients (white circles). Arrows indicate day of treatment. Significance determined by calculating the area under curve of mean disease scores. Graph is representative of $n = 3$ separate experiments with at least $n = 4$ mice per group. (*Middle*) Mean day of EAE onset ± SEM for Tam-B$^{APC}$ mice from the untreated group (blue circles), control serum group (black circles), and anti-CXCR2 recipients (white circles). Data are pooled from $n = 3$ separate experiments with at least $n = 4$ mice per group. Significance determined by Kruskal-Wallis ANOVA test with Dunn's correction for multiple comparisons. $P$ = n.s. for untreated vs. control serum groups, $***P < 0.001$ for untreated vs. anti-CXCR2 groups, and $**P = 0.0096$ for control serum vs. anti-CXCR2 groups. (*Right*) Graph of EAE incidence for Tam-B$^{APC}$ mice from the untreated group (blue line), control serum group (black line), and anti-CXCR2 recipients (dotted black line). Data are pooled from $n = 3$ separate experiments with at least $n = 4$ mice per group. Significance evaluated by log-rank test, $****P < 0.0001$. (*B*) Decalcified Tam-B$^{APC}$ spinal cord stained for (*Left*) B220 (pink), GFAP/podoplanin-1 (green), and DAPI (blue), imaged at 10× magnification. (Scale bars, 100 μm.) (*C*) Peripheral blood B cell expression of MHCII (*Top*) and VLA-4 (*Bottom*) prior to Tam treatment (black histograms) and 72 h post Tam (blue histograms). Plots are representative of at least $n = 10$ mice tested at both time points, pooled from more than 4 independent experiments. (*D*) (*Left*) Mean EAE scores ± SEM; (*Right*) mean day of EAE onset. (*Top*) Graphs of WT (black squares) and Cre-VLA-4$^{f/f}$ (white circles) are representative of 3 independent experiments with $n = 3$ to 11 mice per genotype. (*Center*) Graphs of B$^{MHCII}$xIgH$^{MOG}$ (black squares), B$^{MHCII}$xIgH$^{MOG}$xVLA-4$^{f/+}$ (blue and white circles), and B$^{MHCII}$xIgH$^{MOG}$xVLA-4$^{f/f}$ mice (white circles) are representative of 5 independent experiments with $n = 3$ to 8 mice per genotype. Statistical significance for the day of onset determined by $t$ test. $P$ = n.s. (*Bottom*) Graphs of Tam-B$^{APC}$ mice (blue squares), Tam-B$^{APC}$xVLA-4$^{f/+}$ (blue and white circles), and Tam-B$^{APC}$xVLA-4$^{f/f}$ mice (white circles) are representative of 6 independent experiments with $n = 3$ to 8 mice per genotype. Statistical significance for the day of onset determined by $t$ test. $P$ = n.s.

and heterozygous expression of VLA-4 in B cells were susceptible to EAE with similar severity and day of onset, while mice devoid of B cell VLA-4 expression were completely protected (Fig. 7 *D*, *Bottom*). Examination of spinal cords by immunofluorescence confirmed that Tam-B$^{APC}$ mice and Tam-B$^{APC}$xVLA-4$^{f/+}$ mice with EAE both developed substantial clusters of B cells in the spinal cord meninges, while the deletion of B cell VLA-4 expression prevented B cells from entering the subarachnoid space by extravasation through VCAM-1+ blood vessels (*SI Appendix*, Fig. S4). These results demonstrate the requirement for B cell VLA-4 expression for access to the CNS compartment and antigen presentation function during EAE.

## Discussion

While cognate interactions between B cells and CD4 T cells are known to be important for autoantibody formation in MS, the nature and location of these pathogenic interactions in EAE are unclear. Similarly, the genesis of ELT within the meninges of patients with progressive MS is thought to be clinically relevant, but the mechanisms leading to the formation of these structures remain unknown. We sought to determine the sequence of proinflammatory events that fosters the formation of antigen-specific B and T cell interactions within the CNS intrinsic to the clinicopathologic features of MS. We have found that the subarachnoid space of the spinal cord meninges serves as a niche for B cell cluster formation during EAE. This is corroborated by other reports of ELT in EAE, including Dang et al. (26), who found nonclassically activated B cells in the spinal cord meninges of $TCR^{MOG}xIgH^{MOG}$ mice with spontaneous EAE. In our model, we found a high frequency of MHCII+ B cells that frequently exhibited surface markers such as IgM+ IgD− B cells (27) and naive follicular B cells. The low frequency of CD138+ plasma cells or plasmablasts and few GL7+ GC B cells we observed in the spinal cord meninges can be accounted for by the early time points used in this study. One caveat to these results is that CD138 staining can be challenging based on the lack of stability of this surface marker during processing for flow cytometry, leading to a potential underestimation of the number of plasma cells/plasmablasts. Also, it is important to note that the encephalitogenic donor CD4 T cell lines used to induce passive EAE in our model are very strongly Th1-skewed and thus distinct from models exhibiting ELT in B6 or SJL (Swiss Jim Lambert) mice involving IL-17–skewed CD4 T cells (12, 18). This is relevant, given that prior work has shown that Th17 cells are capable of trafficking to the CNS during EAE without expression of VLA-4 (28). Additionally, donor T cells driving disease in our model may not be capable of functioning as efficient T follicular helper cells to sustain GC reactions. These explanations are not mutually exclusive and deserve further exploration to elucidate the critical mechanisms involved in transitions from immature to established ELT structures in EAE.

To explore the factors recruiting and retaining B cells to the subarachnoid space to the exclusion of other CNS tissues we investigated the kinetics of innate and adaptive immune cell trafficking at several stages of EAE progression. Prior to EAE onset, $CD45^{hi}CD11b^{hi}Gr\text{-}1^{hi}$ PMNs are the most common cell type observed in the spinal cord meninges of Tam-$WT^{APC}$ and Tam-$B^{APC}$ mice. This proinflammatory cell type is often a major component of early inflammatory infiltrates in EAE (22, 29, 30), and it is especially elevated in Tam-$B^{APC}$ mice compared to Tam-$WT^{APC}$ mice. PMNs may be playing a unique role in the early stages of B cell-dependent EAE in which they prime the CNS microenvironment for B cell cluster formation through activating the endothelium or compromising the integrity of the BBB (29, 31). It is possible that PMN transmigration of the BBB results in the up-regulation of VCAM-1 or CXCL13 to promote B cell extravasation into the subarachnoid space. Indeed, peripheral blood isolated from MS patients is enriched for neutrophil extracellular traps (NETs), which are a potent source of antigens and activation signals for autoreactive B cells in systemic lupus erythematosus (SLE) (32–34). Utilizing our unique ability to sample murine CSF, we decided to target CXCR2 as a means of testing our hypothesis that PMN trafficking is essential for B cell recruitment to the spinal cord meninges and initial ELT formation. CXCR2 expression was restricted to PMNs in Tam-$B^{APC}$ mice, and over time, PMNs harvested from the spinal cord meninges of these mice exhibited surface markers indicative of increased activation. We have found that treating Tam-$B^{APC}$ with anti-CXCR2 serum delays the day of EAE onset and resulted in less severe EAE symptoms, consistent with previous studies showing antagonism of CXCR2 signaling protects from neuroinflammation (24, 25, 35). Ameliorated EAE in anti-CXCR2 recipients was associated with complete ablation of B cell clusters in the subarachnoid space as well as changes in the tissue distribution of PMNs. The involvement of PMNs in neuroinflammation, both in MS as well as MS-related diseases, is complex. In our model of B cell-dependent EAE, PMN migration to the CNS is required for B cell antigen presentation function and the development of clinical disease. This does not necessarily indicate that CXCR2-dependent PMN migration is critical to the development of EAE in WT mice due to B cell antigen presentation. Rather, when APC function is isolated to B cells, our data indicate that the process by which B cells accumulate within the meninges is PMN-dependent. Overall, inhibiting the ability of PMNs to respond to timely expression of CXCR2 ligands in our model impedes formation of B cell clusters, potentially due to reductions in PMN-secreted proinflammatory cytokines, less PMN-induced damage to the BBB, and/or inhibited induction of other chemokines that promote the recruitment of other immune cells.

In conclusion, our research indicates that B cell clusters in the spinal cord subarachnoid space are aggregates of immune cells engaging in pathogenic, antigen-specific interactions. Formation of these rudimentary meningeal ELT in Tam-$B^{APC}$ mice is essential for B cell antigen presentation to support neuroinflammation. Prior to the onset of EAE and well before B cell cluster formation, PMNs are recruited to the CNS by ELR+ CXC chemokines. Inhibition of CXCR2-mediated PMN trafficking to the CNS reduces pathogenic B cell clusters, suggesting that PMN recruitment primes the CNS compartment for B cell cluster formation. Therapeutic targeting of CXCR2 signaling could be effective for MS, and more research is needed to investigate the possibility of direct or indirect interactions between PMNs and B cells. In accordance with successful therapies that eliminate B cells (BCDTs) or prevent immune cell trafficking to the CNS (Natalizumab or Fingolimod), B cell-restricted VLA-4 deficiency inhibits the development of EAE symptoms when B cells are the only APCs. Coordinated trafficking of innate and adaptive immune cells may promote EAE by supporting VLA-4–dependent B cell accumulation within the meninges during neuroinflammation. Future experiments aimed at determining whether B cell access to the CNS is necessary for antigen acquisition or presentation to CD4 T cells will be essential in refining cellular immune therapeutic targeting with distinct CNS compartments in mind.

## Materials and Methods

**Mice.** Mice were housed in a single pathogen-free housing facility and fed mouse chow and water ad libitum. Male and female mice between 6 and 10 wk of age were used for all experiments with the exception of the anti-CXCR2 treatment experiments that utilized female mice exclusively. Further information regarding strains and breeding is available in *SI Appendix*.

**EAE.** Passive EAE was induced as previously reported (6) and is described in more detail in *SI Appendix*. For induction of MHCII in vivo, Tam-$WT^{APC}$, Tam-$B^{APC}$, and Tam-$B^{APC}$ x$VLA\text{-}4^{f/f}$ or Tam-$B^{APC}$ x$VLA\text{-}4^{f/+}$ mice were treated with 5 μg Tam (Sigma-Aldrich) in 50 μL corn oil (Sigma-Aldrich) by oral gavage 3 wk after CD4 T cell transfer as described (20). MHCII and VLA-4 expression was verified by flow cytometric analysis of peripheral blood. The Animal Studies Committee/Institutional Animal Care and Use Committee of Washington University in St. Louis approved all animal experiments.

**In Vivo CXCR2 Neutralization.** Rabbit anti-mouse CXCR2 serum was generated according to previous reports (24) and 0.2-μm vacuum-filtered. Control polyclonal rabbit serum (R4505, Sigma-Aldrich) was sterilized with 0.45-μm syringe filters (TPP). Age-matched female Tam-$B^{APC}$ mice were injected intraperitoneally with 200 μL control or anti-CXCR2 serum on days −2, 0, 2, and 4 relative to Tam treatment by oral gavage (at day 0) 3 wk after CD4 T cell transfer. Mice were scored daily for clinical disease and killed 3 d post EAE onset or 13 to 15 d post Tam.

**Flow Cytometry.** Isolation and staining of single cells from various tissues for flow cytometric analysis was preformed according to prior reports (6) and is detailed in *SI Appendix*.

**CSF Collection and Analysis.** Mice were avertin-anesthetized prior to CSF collection from the cisterna magna. CSF was stored in MAXYMum Recovery, low-protein-binding PCR tubes and immediately spun down and frozen. Concentration of cytokines and chemokines was assessed using the BioRad 33-plex kit analyzed on a Luminex. Concentrations of CSF were transformed logarithmically for graphing and statistical analysis purposes.

**Imaging.** Immunofluorescence staining for CD3 and B220 was performed as previously reported (6). Intermittent background labeling from anti-CD3 staining was noted, but consistently within the gray matter and not in a pattern confounding for cellular labeling of T cells. Background immunofluorescence was a result of anti-CD3, as control staining with secondary antibody only never resulted in excessive background signal. Staining for additional markers, including VCAM-1, Ly-6G, podoplanin, and $K_i$-67 is detailed in *SI Appendix*. Optical clearing of spinal cords was initiated by perfusing mice with 25 mL ice-cold phosphate buffered saline followed by 20 mL 4% paraformaldehyde (Sigma-Aldrich). CNS tissue was extracted while still encased in the skull and vertebral column, then fixed in 4% paraformaldehyde for more than 12 h. Spinal cord vertebrae were decalcified in 6% tricholoroacetic acid (Sigma-Aldrich) for 5 d and washed with PBS prior to optical clearing using iDISCO protocol (36). Additional details including confocal imaging are provided in *SI Appendix*.

**Data Availability.** All data discussed in the paper are available via Figshare, https://doi.org/10.6084/m9.figshare.10052051.v1.

**ACKNOWLEDGMENTS.** We thank Denise Dorsey, Christine Pham, Mary Dinauer, and Julia Sim for research advice and Thalia Papayannopoulou at the University of Washington for kindly providing *itga4*$^{f/f}$ mice. We would also like to thank Diane Bender and Michael Shih at Washington University for technical assistance. The National Institute of Neurological Disorders and Stroke supported C.R.P.H. (F31NS096824) and G.F.W. (R01NS106289). Research reported herein was supported by the Immunomonitoring Laboratory within The Andrew M. and Jane M. Bursky Center for Human Immunology and Immunotherapy Programs at Washington University in St. Louis.

1. X. Montalban *et al*.; ORATORIO Clinical Investigators, Ocrelizumab versus Placebo in primary progressive multiple sclerosis. *N. Engl. J. Med.* **376**, 209–220 (2017).
2. S. L. Hauser *et al*.; OPERA I and OPERA II Clinical Investigators, Ocrelizumab versus interferon beta-1a in relapsing multiple sclerosis. *N. Engl. J. Med.* **376**, 221–234 (2017).
3. S. L. Hauser *et al*.; HERMES Trial Group, B-cell depletion with rituximab in relapsing-remitting multiple sclerosis. *N. Engl. J. Med.* **358**, 676–688 (2008).
4. R. T. Naismith *et al*., Rituximab add-on therapy for breakthrough relapsing multiple sclerosis: A 52-week phase II trial. *Neurology* **74**, 1860–1867 (2010).
5. N. Molnarfi *et al*., MHC class II-dependent B cell APC function is required for induction of CNS autoimmunity independent of myelin-specific antibodies. *J. Exp. Med.* **210**, 2921–2937 (2013).
6. C. R. Parker Harp *et al*., B cell antigen presentation is sufficient to drive neuro-inflammation in an animal model of multiple sclerosis. *J. Immunol.* **194**, 5077–5084 (2015).
7. G. Galicia, B. Boulianne, N. Pikor, A. Martin, J. L. Gommerman, Secondary B cell receptor diversification is necessary for T cell mediated neuro-inflammation during experimental autoimmune encephalomyelitis. *PLoS One* **8**, e61478 (2013).
8. G. Disanto *et al*.; Swiss Multiple Sclerosis Cohort Study Group, Serum neurofilament light: A biomarker of neuronal damage in multiple sclerosis. *Ann. Neurol.* **81**, 857–870 (2017).
9. B. Serafini, B. Rosicarelli, R. Magliozzi, E. Stigliano, F. Aloisi, Detection of ectopic B-cell follicles with germinal centers in the meninges of patients with secondary progressive multiple sclerosis. *Brain Pathol.* **14**, 164–174 (2004).
10. R. Magliozzi *et al*., Meningeal B-cell follicles in secondary progressive multiple sclerosis associate with early onset of disease and severe cortical pathology. *Brain* **130**, 1089–1104 (2007).
11. R. Magliozzi, S. Columba-Cabezas, B. Serafini, F. Aloisi, Intracerebral expression of CXCL13 and BAFF is accompanied by formation of lymphoid follicle-like structures in the meninges of mice with relapsing experimental autoimmune encephalomyelitis. *J. Neuroimmunol.* **148**, 11–23 (2004).
12. A. Peters *et al*., Th17 cells induce ectopic lymphoid follicles in central nervous system tissue inflammation. *Immunity* **35**, 986–996 (2011).
13. S. Kuerten *et al*., Tertiary lymphoid organ development coincides with determinant spreading of the myelin-specific T cell response. *Acta Neuropathol.* **124**, 861–873 (2012).
14. J. R. Avasarala, A. H. Cross, J. L. Trotter, Oligoclonal band number as a marker for prognosis in multiple sclerosis. *Arch. Neurol.* **58**, 2044–2045 (2001).
15. M. Haugen, J. L. Frederiksen, M. Degn, B cell follicle-like structures in multiple sclerosis-with focus on the role of B cell activating factor. *J. Neuroimmunol.* **273**, 1–7 (2014).
16. O. W. Howell *et al*., Meningeal inflammation is widespread and linked to cortical pathology in multiple sclerosis. *Brain* **134**, 2755–2771 (2011).
17. K. Lehmann-Horn, S. A. Sagan, C. C. Bernard, R. A. Sobel, S. S. Zamvil, B-cell very late antigen-4 deficiency reduces leukocyte recruitment and susceptibility to central nervous system autoimmunity. *Ann. Neurol.* **77**, 902–908 (2015).
18. N. B. Pikor *et al*., Integration of Th17- and lymphotoxin-derived signals initiates meningeal-resident stromal cell remodeling to propagate neuroinflammation. *Immunity* **43**, 1160–1173 (2015).
19. M. S. Weber *et al*., B-cell activation influences T-cell polarization and outcome of anti-CD20 B-cell depletion in central nervous system autoimmunity. *Ann. Neurol.* **68**, 369–383 (2010).
20. C. R. Parker Harp *et al*., B cells are capable of independently eliciting rapid re-activation of encephalitogenic CD4 T cells in a murine model of multiple sclerosis. *PLoS One* **13**, e0199694 (2018).
21. C. Caravagna *et al*., Diversity of innate immune cell subsets across spatial and temporal scales in an EAE mouse model. *Sci. Rep.* **8**, 5146–5163 (2018).
22. A. L. Christy, M. E. Walker, M. J. Hessner, M. A. Brown, Mast cell activation and neutrophil recruitment promotes early and robust inflammation in the meninges in EAE. *J. Autoimmun.* **42**, 50–61 (2013).
23. C. Allen *et al*., Neutrophil cerebrovascular transmigration triggers rapid neurotoxicity through release of proteases associated with decondensed DNA. *J. Immunol.* **189**, 381–392 (2012).
24. T. Carlson, M. Kroenke, P. Rao, T. E. Lane, B. Segal, The Th17-ELR+ CXC chemokine pathway is essential for the development of central nervous system autoimmune disease. *J. Exp. Med.* **205**, 811–823 (2008).
25. S. B. Simmons, D. Liggitt, J. M. Goverman, Cytokine-regulated neutrophil recruitment is required for brain but not spinal cord inflammation during experimental autoimmune encephalomyelitis. *J. Immunol.* **193**, 555–563 (2014).
26. A. K. Dang, Y. Tesfagiorgis, R. W. Jain, H. C. Craig, S. M. Kerfoot, Meningeal infiltration of the spinal cord by non-classically activated B cells is associated with chronic disease course in a spontaneous B cell-dependent model of CNS autoimmune disease. *Front. Immunol.* **6**, 470–482 (2015).
27. F. J. Weisel, G. V. Zuccarino-Catania, M. Chikina, M. J. Shlomchik, A temporal switch in the germinal center determines differential output of memory B and plasma cells. *Immunity* **44**, 116–130 (2016).
28. V. Rothhammer *et al*., Th17 lymphocytes traffic to the central nervous system independently of α4 integrin expression during EAE. *J. Exp. Med.* **208**, 2465–2476 (2011).
29. B. Aubé *et al*., Neutrophils mediate blood-spinal cord barrier disruption in demyelinating neuroinflammatory diseases. *J. Immunol.* **193**, 2438–2454 (2014).
30. J. M. Rumble *et al*., Neutrophil-related factors as biomarkers in EAE and MS. *J. Exp. Med.* **212**, 23–35 (2015).
31. C. S. Casserly, J. C. Nantes, R. F. Whittaker Hawkins, L. Vallières, Neutrophil perversion in demyelinating autoimmune diseases: Mechanisms to medicine. *Autoimmun. Rev.* **16**, 294–307 (2017).
32. J. S. Knight, M. J. Kaplan, Lupus neutrophils: 'NET' gain in understanding lupus pathogenesis. *Curr. Opin. Rheumatol.* **24**, 441–450 (2012).
33. N. Gestermann *et al*., Netting neutrophils activate autoreactive B cells in lupus. *J. Immunol.* **200**, 3364–3371 (2018).
34. K. H. Lee *et al*., Neutrophil extracellular traps (NETs) in autoimmune diseases: A comprehensive review. *Autoimmun. Rev.* **16**, 1160–1173 (2017).
35. A. E. Kerstetter, D. A. Padovani-Claudio, L. Bai, R. H. Miller, Inhibition of CXCR2 signaling promotes recovery in models of multiple sclerosis. *Exp. Neurol.* **220**, 44–56 (2009).
36. N. Renier *et al*., iDISCO: A simple, rapid method to immunolabel large tissue samples for volume imaging. *Cell* **159**, 896–910 (2014).